

Investigation of Anticorrosion, Antibacterial and *In Vitro* Biological Performance of Terbium / Gadolinium Dual Substituted Hydroxyapatite Coating on Surgical Grade Stainless Steel for Biomedical Applications

C. SRIDEVI^{1,3}, S. SATHISHKUMAR², S. ELAVARASAN²
R. RAJAVEL³ and P. MAHESWARAN^{1*}

¹Department of Chemistry, PGP College of Arts and Science, Namakkal-637 207, Tamilnadu, India

²Synthetic Organic Chemistry Laboratory, Department of Chemistry, Sri Vijay Vidyalaya College of Arts and Science, Dharmapuri, Tamilnadu, India.

³Department of Chemistry, Periyar University, Salem-636 011, Tamilnadu, India
sathish.sskg@gmail.com

Received 17 November 2017 / Accepted 12 December 2017

Abstract: Development of terbium/gadolinium dual substituted hydroxyapatite on 316L stainless steel (SS) have been studied. The coatings were characterized by Fourier transform infrared spectroscopy (FT-IR), X-ray diffraction (XRD), scanning electron microscopy (SEM) and energy dispersive X-ray analysis (EDAX). The electrochemical results show that the Tb/Gd-HAP coating on 316L SS possesses greatest corrosion resistance in Ringer's solution. The antimicrobial performance was studied for the obtained coatings against the pathogenic bacterial strains *S. aureus* and *E. coli*. The *in vitro* cell adhesion test revealed that the Tb/Gd-HAP coating was found appropriate for the formation of new cell growth which proves the enhanced biocompatible nature of the coating. Thus, the Tb/Gd-HAP coating on 316L SS can play a key role in the biomedical applications.

Keywords: Tb and Gd-HAP, 316L SS, Antibacterial activity, Corrosion resistance, Bioactivity

Introduction

Metallic biomaterials such as cobalt alloys, titanium alloys, 316L stainless steel (SS) and magnesium alloys are mostly used as orthopedic implants due to their good strength and toughness¹⁻⁴. However, there is for all time a concern about their corrosion resistance in physiological medium and their good biocompatibility. Austenitic stainless steels are used hugely as human body implants due to availability at low cost, ease of fabrication, excellent

processability and better mechanical properties⁵⁻⁸. The metal surface of austenitic stainless steel is prone to release iron, chromium, nickel ions evidenced in the human body⁹⁻¹¹. Leached nickel and chromium ions are toxic species and powerful allergens and demonstrated to be carcinogenic. In this regard, decrease in metal ion release is preferred to avoid the harmful effect caused by the corrosion products in the bone formation. In order to overcome the metal ion release, the bioactive and osteointegrated bioceramic coatings especially hydroxyapatite [$\text{Ca}_{10}(\text{PO}_4)_6(\text{OH})_2$, HAP] was developed on the surface of the implant material¹²⁻¹⁶. Hydroxyapatite widely used as repair materials for bone because of its likeness in chemical composition to the inorganic matrix of the bones and tissues in mammals. The properties of hydroxyapatite were particular to be controlled by its crystal structure and composition. Therefore the substitution of Ca^{2+} with other metal ions (Zn, Tb, Sm, Ce, Eu, etc...) plays an essential role in the improvement of biological performance of hydroxyapatite¹⁷⁻²⁴. In particular, Terbium ions plays a major role in improving the biocompatibility and biodegradability of hydroxyapatite bioceramics which enhances the *in vitro* and *in vivo* osteoblast cell proliferation and growth. On the other hand, the improved anticorrosion performance of the implant materials should be considered for superior biological activities²⁵. Gadolinium is one of the significant trivalent ions in lanthanide series with good anticorrosion behavior²⁶. In addition, Gd ions are used as the drug carrier and anticancer agent and the presence of Gd induces the osteoconductivity and cell enlargement. Majeed *et al.* have previously reported the preparation of Gd_2O_3 and $\text{Eu}:\text{Gd}_2\text{O}_3$ nanocrystals and among them Gd_2O_3 nanopowders were found to be biologically biocompatible by the cell proliferation test²⁷. In present work we achieved the development of Terbium/Gadolinium dual substituted hydroxyapatite on 316L SS. The coatings were characterized by Fourier transform infrared spectroscopy (FT-IR), x-ray diffraction (XRD), scanning electron microscopy (SEM) and energy dispersive x-ray analysis (EDAX). The electrochemical results show that the Tb/Gd-HAP coating on the passivated 316L SS possesses greatest corrosion resistance in Ringer's solution. The antimicrobial performance was studied for the obtained coatings against the pathogenic bacterial strains *S. aureus* and *E. coli* and also the *in vitro* cell viability test was performed using MC3T3-E1 cell lines to estimate the bioactivity of the coating. Thus, the Tb, Gd-HAP coating on 316L SS will serve as a promising candidate with improved corrosion resistance, antibacterial property and osteocompatibility.

Experimental

Type 316L SS (procured from Steel Authority of India, Ltd. (SAIL), India), having an elemental composition (wt %) of 0.0222 C, 0.551 Si, 1.67 Mn, 0.023 P, 0.0045 S, 17.05 Cr, 11.65 Ni, 2.53 Mo, 0.136 Co, 0.231 Cu, 0.0052 Ti, 0.0783 V, 0.0659 N and Fe (balance), was used as the metal substrate for the electrodeposition. The 316L SS substrate with a size of $10 \times 10 \times 3$ mm were embedded in epoxy resin, leaving an area of 1 cm^2 for exposure to the electrolyte solution. Prior to electrodeposition, these substrates were abraded with different grades of silicon carbide (SiC) emery papers from 400 grit to 1200 grit. After polishing, these samples were ultrasonically cleaned and thoroughly washed with acetone and deionized water for 10 min and finally, rinsed in deionized (DI) water and dried. In order to improve the anticorrosion property, the 316L SS surface was passivated using 0.4 M borate buffer solution (pH 9.3) at 640 mV vs. saturated calomel electrode (SCE) for 2 h in potentiostatic condition using electrochemical workstation (Model CHI 760C, CH Instruments, USA).

Preparation of electrolyte solution

The electrolyte solution for Tb,Gd-HAP were prepared by dissolving analytical grade 0.3 M calcium nitrate hexahydrate ($\text{Ca}(\text{NO}_3)_2 \cdot 6\text{H}_2\text{O}$), 0.1 M Terbium nitrate hexahydrate ($\text{Tb}(\text{NO}_3)_3 \cdot 6\text{H}_2\text{O}$) and 0.1 M Gadolinium nitrate hexahydrate ($\text{Gd}(\text{NO}_3)_3 \cdot 6\text{H}_2\text{O}$) in (DI) deionized water. The 0.3 M diammonium hydrogen phosphate ($(\text{NH}_4)_2\text{HPO}_4$) solution was dissolved in deionized water and the solution was mixed with (Ca + Tb + Gd)/P molar ratio of 1.67 at room temperature (28 ± 1 °C). Then the solution was under magnetic stirring for 4 h and the pH of the electrolyte was adjusted to 4.7 using ammonia hydroxide solution. All the chemicals were analytic grade reagents (purchased from sigma Aldrich) and used without further purification.

Electrodeposition of Tb, Gd-HAP

The Tb, Gd-HAP coating on 316L SS was carried out in three different constant cathodic potentials of -1200, -1400 and -1600, mV vs. SCE for the time of 1 h in potentiostatic mode by maintaining the temperature at 50 °C. After the electrodeposition the coating substrates were gently rinsed with deionized water, dried in the air and then stored in a desiccators for additional studies.

Surface characterization

The Tb, Gd-HAP coating materials were analyzed using Fourier transform infrared spectroscopy (FT-IR) using a Bruker Tensor²⁷. The FT-IR spectra were recorded from 4000-400 cm^{-1} with the region of 4 cm^{-1} resolution by using the KBr pellet technique method. The crystallinity structure of coated samples was investigated by x-ray diffraction PANalytical X'Pert PRO diffractometer in the 2θ angle between 20° - 60° with Cu K α radiation (1.5406 Å). The surface morphology and elemental composition of as a developed duplex layer coating were evaluated by a high resolution scanning electron microscopy (HRSEM, JSM 840A, JEOL-Japan) equipped with EDAX.

Antibacterial activity

The antibacterial activity of the Tb/Gd-HAP coating at different concentrations have been investigated against two bacterial strains *S. aureus* (ATCC 25923) and *E. coli* (ATCC 25922) via agar disc diffusion method. The Mullar-Hinton agar plates were prepared by pouring 15 mL of a molten medium into sterile Petri plates. The plates were allowed to solidify for ~15 min and 0.1% of inoculum suspension was swabbed uniformly over the agar until the inoculum became invisible. Different concentrations (25, 50, 75, 100 and 125 μL) of Tb,Gd-HAP coating were loaded onto 5 mm sterile individual discs, followed by incubation of plates at 37 °C for 24 h. The zone of inhibition was observed by measuring the width of the inhibited zone.

Osteocompatibility studies

The cell proliferation of MC3T3-E1 cells on Tb/Gd-HAP was studied using MTT assay on day 1, 3 and 5. To determine the cytotoxicity of the samples at different conditions, MC3T3-E1 cells were seeded in 12-well plates at 104 cells/mL in a humidified 5% CO_2 atmosphere. Each time, 400 μL of MTT reagent (1 mg/mL) was added to each well and incubated for 4 h under the same conditions. Finally, MTT reagent was removed and 400 μL of dimethyl sulfoxide (DMSO, Sigma-Aldrich) was added for dissolving the formazan crystals and the absorbance was measured at 560 nm in an ELISA microplate reader and then the cell viability (as a percentage) was calculated, with respect to the control, as follows:

$$\% \text{ Cell viability} = [\text{A}] \text{ Test} / [\text{A}] \text{ Control} \times 100$$

Results and Discussion

FT-IR Analysis

The FTIR spectrum of Tb/Gd-HAP coating on 316L SS sample is shown in Figure 1. The characterized peaks at 472 cm^{-1} , 588 cm^{-1} , 602 cm^{-1} as well as the peaks attributed in 874 cm^{-1} and 961 cm^{-1} were assigned in the phosphate group in Tb/Gd-HAP. The sharp peaks at 1091 cm^{-1} and 1025 cm^{-1} were due to the asymmetric stretching of P-O bond of phosphate groups. In addition, absorption bands at 3572 cm^{-1} and 633 cm^{-1} are due to the stretching and bending vibration of OH^- groups of Tb,Gd -HAP, respectively. The broad band at 3427 cm^{-1} and a peak at 1624 cm^{-1} are assigned for the stretching and bending mode of the H_2O molecules. Thus, the FTIR spectrum clearly evidenced the formation of Tb,Gd-HAP coating on 316L SS.

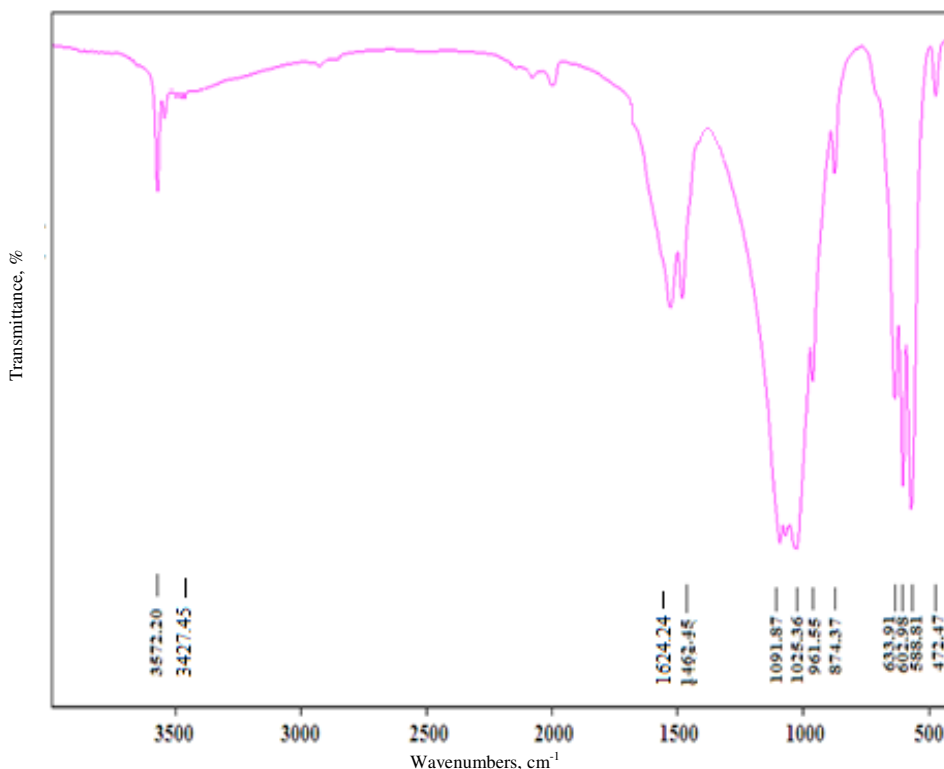


Figure 1. FT-IR spectra of Tb,Gd-HAP coating on 316 L SS

X-Ray diffraction studies

The XRD pattern of as developed Tb,Gd-HAP coating on 316L SS is shown in Figure 2. The strong diffraction peaks detected for Tb,Gd-HAP are in well agreement with the standard data for HAP (ICDD card No. 09-0432). The main diffraction peaks (Figure 2) are indicated at 2θ values of 25.6° , 31.5° , 32.2° , 32.8° , 34.6° , 39.8° , 46.6° and 53.1° corresponds to Tb, Gd-HAP and no other secondary peaks were detected. Moreover, the intense diffraction peaks resembles the high crystalline nature of the Tb,Gd-HAP coating as evidenced in the Figure 2.

Morphological investigations

The surface morphology of Tb,Gd-HAP coatings on 316L SS at variation voltages of -1200 mV, -1400 mV and -1600 mV are showed Figure 3(a-c). The morphological feature of non uniform and not surface covered coating at -1200 mV shown in the Figure 3a. The Tb, Gd-HAP coatings obtained at -1400 mv (Figure 3b) produces the fully covered rod like morphology of compare then -1200 mV (Figure 3a) and -1600 mV (Figure 3c). Hence, Figure 3b (-1400 mV) shows fully covered rod like structure and fixed the optimal condition of Tb, Gd-HAP coating on 316L SS. Figure 3d shows the EDAX spectrum of the Tb, Gd-HAP coated on 316 L SS. This spectrum indicates the presence of Ca, Gd, Tb, O and P there by confirms the existence of Tb,Gd-HAP coating on 316L SS.

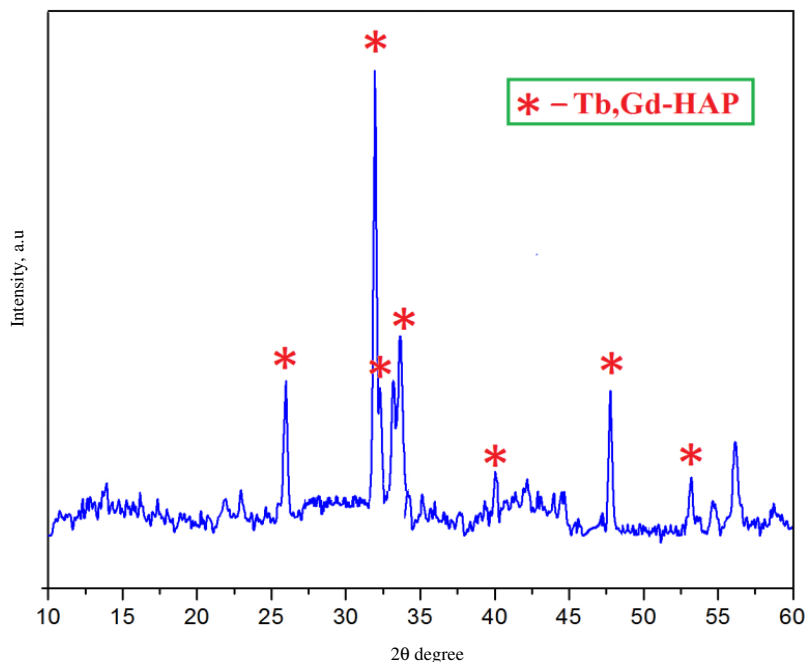
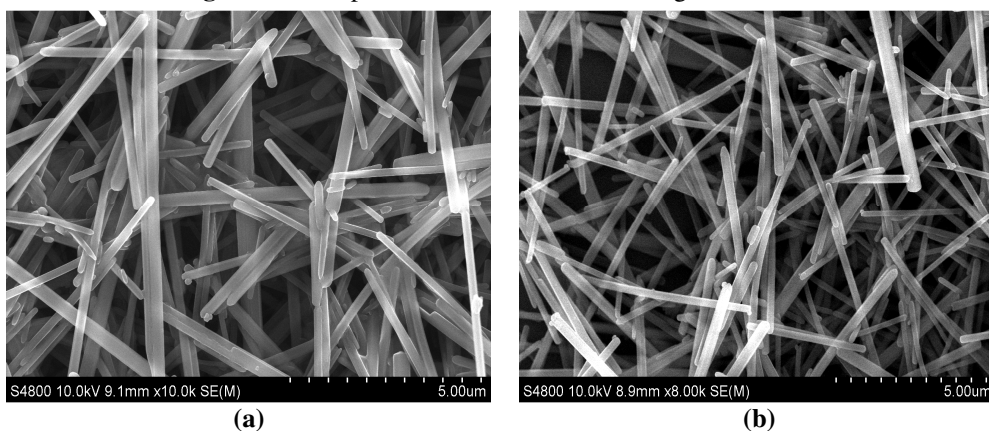
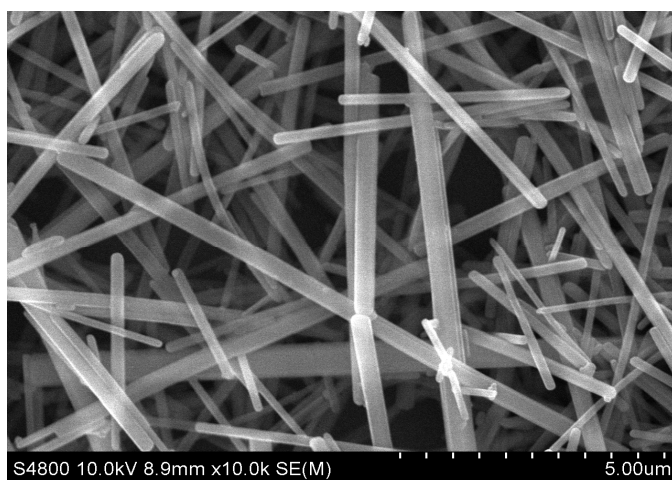


Figure 2. XRD patterns of Tb,Gd-HAP coating on 316 L SS





(c)

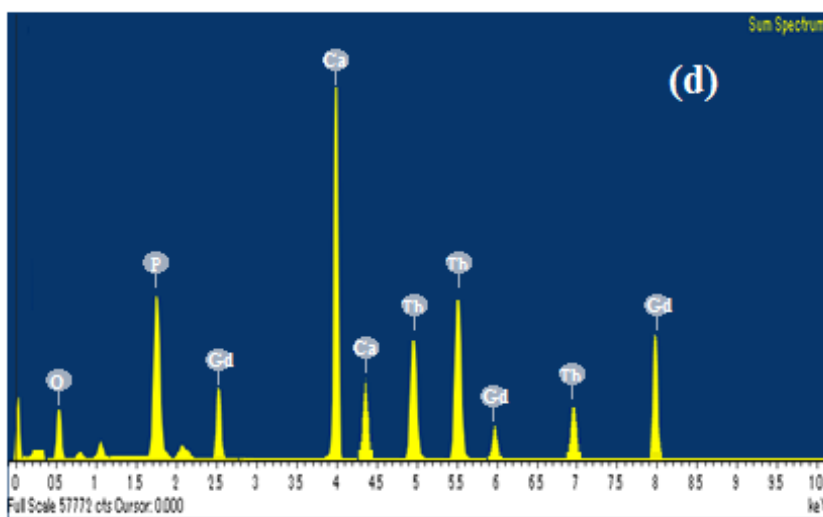


Figure 3. SEM micrographs of (a) Tb,Gd-HAP -1200 mV, (b) Tb,Gd-HAP -1400 mV, (c) Tb,Gd-HAP -1600 mV coatings on 316L SS. (d) EDAX spectrum of the Tb,Gd-HAP coating on 316L SS

Electrochemical studies

The potentiodynamic polarization curves of uncoated, HAP coated and Tb,Gd-HAP coated on 316L SS in Ringer solution are shown in Figure 4. As indicated from the Figure (4a) corrosion potential (E_{corr}), breakdown potential (E_b) and repassivation potential (E_{pp}) for the uncoated 316L SS were found to be at -865, +447 and -88 mV vs. SCE, respectively. However, HAP coated samples the E_{corr} , E_b and E_{pp} values were found to be -790, +502 and 185 mV vs. SCE, respectively. While the polarization parameter of Tb, Gd-HAP coated on 316L SS shows values of $E_{\text{corr}} = -662$, $E_b = +617$ and $E_{\text{pp}} = 213$ mV vs. SCE, respectively. When compared with the uncoated and HAP coated 316L SS, the E_{corr} , E_b and E_{pp} values of the Tb, Gd-HAP coated samples showed maximum shift towards the nobler direction.

The Impedance spectroscopic studies of uncoated, HAP coated, Tb, Gd-HAP coated on 316L SS samples are shown in Figure 4b. The polarization resistance (R_p) of the Tb,Gd-HAP coating on 316L SS, which better polarization resistance (R_p) of 1669 $\Omega \text{ cm}^2$, which is higher than that obtained for the HAP coated on 316L SS (796 $\Omega \text{ cm}^2$) and uncoated 316L SS (45 $\Omega \text{ cm}^2$). The E_{corr} , E_b , E_{pp} and R_p values towards the noble direction is an indicated that the Tb, Gd-HAP coating possessed superior anti corrosion performance in Ringers solution.

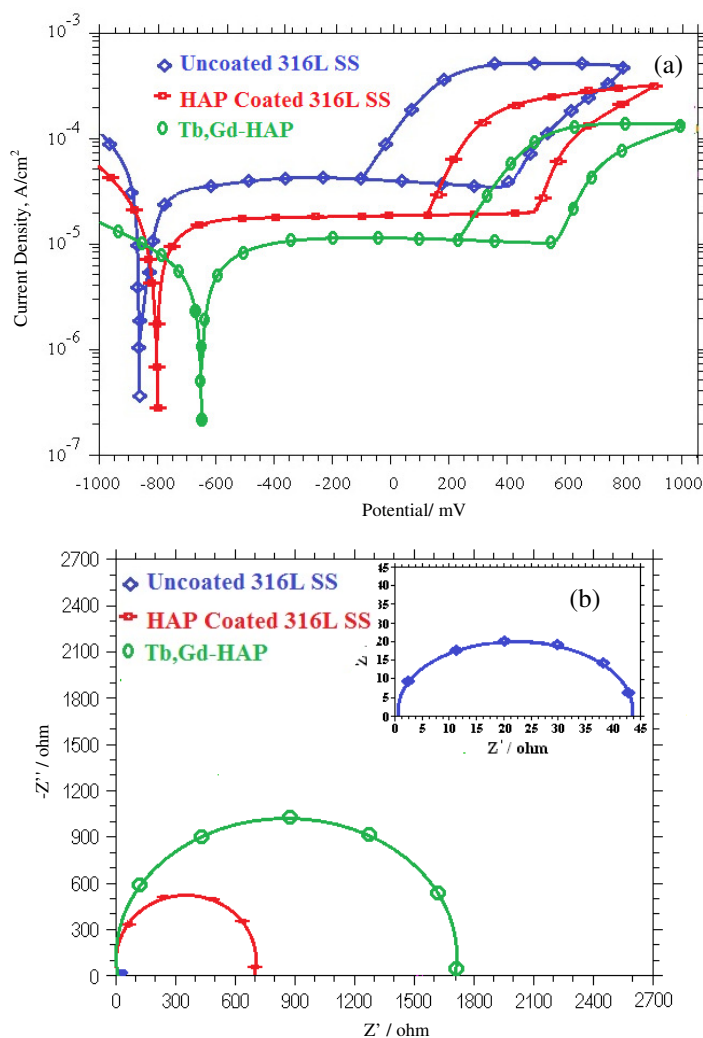


Figure 4. Electrochemical parameters of Tb, Gd-HAP coating on 316L SS
(a) potentiodynamic polarization curve and (b) Bode impedance plot

Antibacterial Activity

The antibacterial efficacy of the Tb, Gd-HAP coating at different concentrations was tested at against the pathogenic bacteria *S. aureus* (Gram-positive bacteria) and *E. coli* (Gram negative bacteria) by the disc diffusion method. The zone of inhibition around the Tb,Gd-HAP samples at various concentrations (25, 50, 75, 100 and 125 mL) against *E. coli* and *S. aureus* is

indicated in Figure 5. The two prokaryotic strains of zone inhibition over the Tb, Gd-HAP coating was higher upon the increase of sample concentrations, when compared with control. In specifically, the action of the Tb, Gd-HAP coating against the negative bacteria (*E. coli*) strain was slightly higher when compared to that of Gram-positive bacteria (*S. aureus*). In this figure, the asterisk symbol (*) denotes a significant difference compared to control ($P < 0.05$).

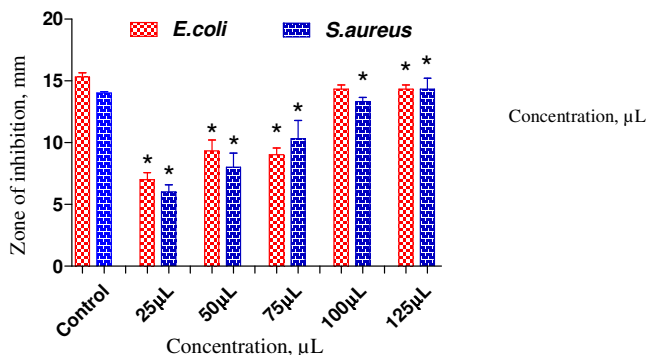


Figure 5. Antimicrobial activities of Tb,Gd-HAP coatings at different concentrations against pathogenic bacteria *S. aureus* and *E. coli*. The asterisk (*) denotes a significant difference compared to control ($P < 0.05$)

Live/Dead assay

The cell proliferation of MC3T3-E1 cells on the Tb, Gd-HAP coated samples was determined using a MTT assay for 1, 3, 5 and 7 days of culture and the results are indicated in Figure 6. The evaluation of live/dead cells was carry out by culturing in medium for 1, 3, 5 and 7 days. The fluorescent microscopic images demonstrating the green are live cells, calcein acetomethylester (AM) was used for green. The number of live cells is increased and spreading elongated morphology as the incubation time increases. Although comparing the various days (1,3,5 and 7) the Tb, Gd-HAP coating exhibited superior cell proliferation and elongated morphology on 7 day, compared with other days (1,3,5) of culture and control (Figure 7).

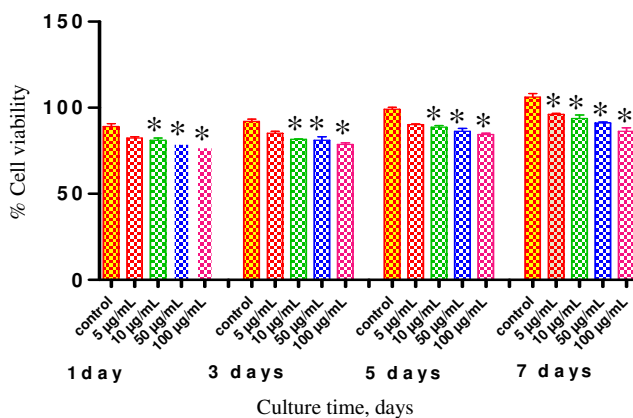


Figure 6. Cytotoxicity analysis of Tb,Gd-HAP coatings on MC3T3-E1 cells for 1, 3, 5 and 7 days. The asterisk symbol (*) denotes a significant difference, compared to control ($P < 0.05$)

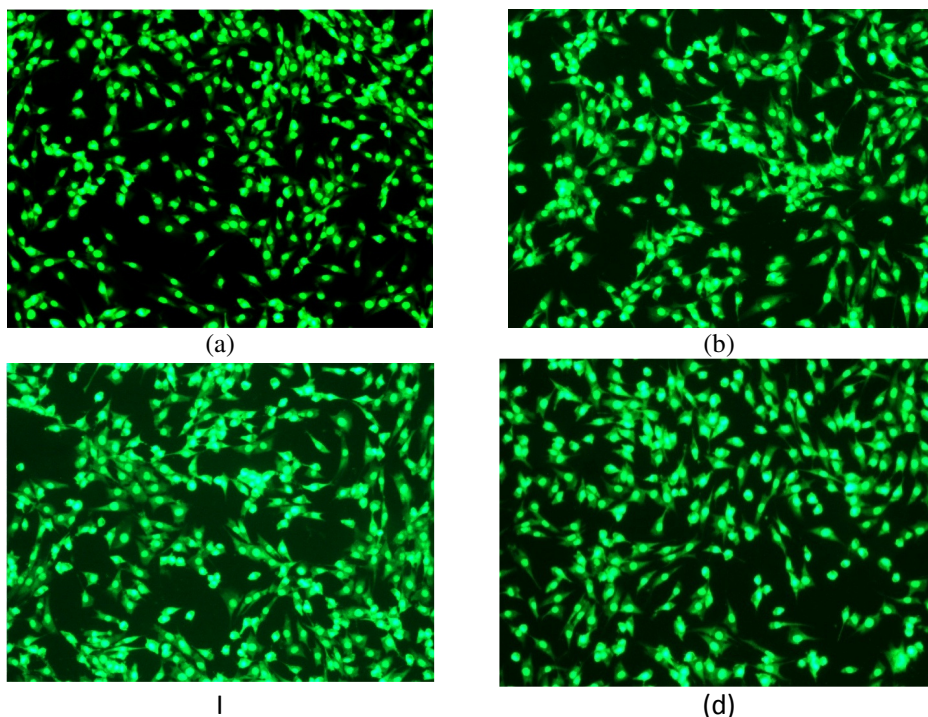


Figure 7. Live/dead cells fluorescence micrographs of osteoblasts cultured on Tb, Gd-HAP coating for (a) control, (b) 1 day, (c) days and (d) 7 days.

Conclusion

The development of Tb, Gd-HAP coating on 316L SS was successfully achieved by electrochemical deposition method. The FT-IR and XRD investigations confirmed the functional groups and phase purity of the Tb, Gd-HAP coating on 316L SS. The surface morphological results indicated that the Tb, Gd-HAP coating achieved on 316L SS with uniform surface fully covered rods. Hence, the electrochemical evaluations showed that the Tb, Gd-HAP coating exhibited superior anticorrosion properties in Ringers solution. The as formed Tb, Gd-HAP coating possessed a better antibacterial property. The *in vitro* biocompatibility analysis indicate that the Tb, Gd-HAP coating promotes the cell viability and proliferation of the MC3T3-E1 cells. Thus, the Tb, Gd-HAP coating on 316L SS can be an choice implant material with enhanced properties for biomedical applications.

References

1. Hornberger H, Virtanen S and Boccaccini A R, *Acta Biomater.*, 2012, **8(7)**, 2442-2455; DOI:10.1016/j.actbio.2012.04.012
2. Bavya Devi K, Singh K and Rajendran N, *J Sol-Gel Sci Technol.*, 2011, **59(3)**, 513; DOI:10.1007/s10971-011-2520-x
3. Proskurovsky D I, Rotshtein V P, Ozur G E, Markov A B, Nazarov D S, Shulov V A, Yu F, Ivanov R and Buchheit G, *J Vac Sci Technol A*, 1998, **16**, 2480; DOI:10.1116/1.581369
4. Huo H, Ying L and Wang F, *J Mater Sci Technol.*, 2007, **23(3)**, 379-382.

5. Afzal M A F, Kalmodia S, Kesarwani P, Basu B and Balani K, *J Biomater Appl.*, 2013, **27(8)**, 967-978.
6. Tang Y, Katsuma S, Fujimoto S and Hiromoto S, *Acta Biomater.*, 2006, **2(6)**, 709-715; DOI:10.1016/j.actbio.2006.06.003
7. Kluba A, Bociaga D and Dudek M, *Diamond Relat Mater.*, 2010, **19(5-6)**, 533-536; DOI:10.1016/j.diamond.2009.12.020
8. Sridhar T M, Kamachi Mudali U, Subbaiyan M, *Corros Sci.*, 2003, **45(10)**, 2337-2359; DOI:10.1016/S0010-938X(03)00063-5
9. Javid M, Javadpour S, Bahrololoom M E and Ma J *Mater Sci Engg C*, 2008, **28(8)**, 1509-1515; DOI:10.1016/j.msec.2008.04.003
10. Sivakumar M and Rajeswari S, *J Mater Sci Lett.*, 1992, **11(15)**, 1039-1042; DOI:10.1007/BF00729754
11. Ballarre J, Lopez D A, Schreiner W H, Duran A and Cere S M, *Appl Surf Sci.*, 2007, **253(17)**, 7260-7264; DOI:10.1016/j.apsusc.2007.03.007
12. Wen C, Guan S, Peng L, Ren C, Wang X and Hu Z, *Appl Surface Sci.*, 2009, **255(13-14)**, 6433-6438; DOI:10.1016/j.apsusc.2008.09.078
13. Matsunaga K, Murata H, Mizoguchi T and Nakahira A, *Acta Biomaterialia*, 2010, **6(6)**, 2289-2293; DOI:10.1016/j.actbio.2009.11.029
14. Zheng X, Huang M and Ding C, *Biomaterials*, 2000, **21(8)**, 841-849; DOI:10.1016/S0142-9612(99)00255-0
15. Geng F, Tan L L, Jin X X, Yang J Y and Yang K, *J Mater Sci Mater Med.*, 2009, **20**, 1149-1157; DOI:10.1007/s10856-008-3669-x
16. Yang Y, Kim K H and Ong J L, *Biomaterials*, 2005, **26(3)**, 327-337; DOI:10.1016/j.biomaterials.2004.02.029
17. Serre C M, Papillard M, Chavassieux P, Voegel J C and Boivin G, *J Biomed Mater Res.*, 1998, **42(4)**, 626-633; DOI:10.1002/(SICI)1097-4636(19981215)42:4<626::AID-JBM20>3.0.CO;2-S
18. Morais D S, Coelho J, Ferraz M P, Gomes P S, Fernandes M H, Hussain N S, Santos J D and Lopes M A, *J Mater Chem B*, 2014, **2**, 5872-5888; DOI:10.1039/C4TB00484A
19. Ciobanu C S, Popa C L and Predoi D, *J Nanomater.*, 2014, 780686; DOI:10.1155/2014/780686
20. Yang C, Yang P, Wang W, Gai S, Wang J, Zhang M and Lin J, *J Coll Int Sci.*, 2008, **328(1)**, 203-210; DOI:10.1016/j.jcis.2008.09.010
21. Yingguang L, Zhuoru Y and Jiang C, *J Rare Earths*, 2007, **25(4)**, 452-456; DOI:10.1016/S1002-0721(07)60455-4
22. Shang H B, Chen F, Wu J, Qi C, Lu B Q, Chen X and Zhu Y J, *RSC Adv.*, 2014, **4**, 53122-53129. DOI:10.1039/C4RA09902H
23. Escudero A, Calvo M E, Fernández S R, de la Fuente J M and Ocanna M, *Langmuir*, 2013, **29(6)**, 1985-1994; DOI:10.1021/la304534f
24. Chen F, Huang P, Zhu Y J, Wu J, Zhang C L and Cu D X, *Biomaterials*, 2011, **32**, 9031-9039; DOI:10.1016/j.biomaterials.2011.08.032
25. Li L, Liu Y, Tao J, Zhang M, Pan H, Xu X and Tang R, *J Phys Chem C*, 2008, **112(32)**, 12219-12224; DOI:10.1021/jp8026463
26. El'kin O V and Kovalevskii A V, *Russ J Electrochem.*, 2011, **47(7)**, 865-868; DOI:10.1134/S1023193511070068
27. Majeed S and Shivashankar S A, *J Mater Chem B*, 2014, **2**, 5585-5593; DOI:10.1039/C4TB00763H